PCCP

Accepted Manuscript

ROYAL SOCIETY OF CHEMISTRY

www.rsc.org/pccp

Molecular design of electron transport with orbital rule: toward conductance-decay free molecular junctions

Tomofumi Tada*,† and Kazunari Yoshizawa*,‡

†*Materials Research Center for Element Strategy, Tokyo Institute of Technology, 4259 Nagatsuta, Midori-ku, Yokohama 226-8503, Japan, E-mail: tada.t.ae@m.titech.ac.jp*

‡*Institute for Materials Chemistry and Engineering, Kyushu University, Nishi-ku, Fukuoka 819-0395, Japan, E-mail: kazunari@ms.ifoc.kyushu-u.ac.jp*

In this Perspective we report our way of thinking about single molecular conductance in terms of frontier orbitals. The orbital rule derived from orbital phase and amplitude is a powerful guideline for the qualitative understanding of molecular conductance in both theoretical and experimental studies. The essence of the orbital rule is the phase-related quantum interference, and on the basis of this rule a constructive or destructive pathway for electron transport is easily predicted. We have worked for the construction of the orbital rule for more than ten years and recently found from its application that π-stacked molecular junctions fabricated experimentally are in line with the concept for conductance-decay free junctions. We explain the orbital rule using the benzene molecular junctions with the *para*-, *meta*- and *ortho*-connections and discuss linear π-conjugated chains and π-stacked molecular junctions with respect to their small decay factors in this manuscript.

Introduction

Since the theoretical proposal of single molecular device by Aviram and Ratner,[1] the electron transport in metal-molecule-metal junctions (i.e., single molecular junctions) has attracted much attention for possible applications of molecular wire, memory and diode in mind.[2-5] Although single molecular device is still a "future nano device" of dream, experimental measurements with scanning probes and theoretical calculations have deepened our understanding of basic electron transport properties through single molecules between electrodes. The Landauer formula[6] with the nonequilibrium Green's function (NEGF) techniques[7] is of great use for theoretical consideration of electron transport phenomena in metal-molecule-metal junctions. Several important mechanisms that determine fundamental aspects of the conductance of a single molecular junction have been discussed as a function of molecular length, molecular conformation and applied bias voltage.[8-16] The conduction channel analysis in terms of molecular orbital (MO) delocalization near the Fermi energy of electrodes has shown good guidelines to understand the electronic properties of molecules between electrodes. The NEGF method[7,17-19] combined with density functional theory (DFT)[20,21] is a popular method at present for calculating coherent electron transmission probability.[22-24] Molecular orbital analysis based on NEGF-DFT calculations revealed that the delocalization of specific MOs is important to make a good conduction pathway,[17,25-27] although DFT Kohn-Sham orbitals and molecular orbitals as the approximate solutions of the Schrödinger equation show qualitative similarity, but the correlations between them are at best indirect.[28,29] On the other hand, the exponential decrease of conductance as a function of molecular length is found to be essential in single molecular junctions,[2,10] which is also

related to orbital delocalization. Thus, there is a tradeoff relation between high conductance from orbital delocalization and exponential decay also from orbital delocalization.

A simple electronic structure model is of great use to develop our intuitive understanding in comparison with a quantitative one, in general. Thus, we have carefully investigated a relationship between frontier orbitals and electron transport properties of π-conjugated systems,[30-40] where frontier orbitals mean the highest occupied molecular orbital (HOMO) and lowest unoccupied molecular orbital (LUMO). The derived rule describes the importance of the phase and amplitude of HOMO and LUMO to determine essential features of the electron transport in molecules. The orbital rule was derived by means of Green's function for the molecular part of a metal-molecule-metal junction assuming a weak contact between a molecule and gold chains (i.e., electrodes). By looking at the phase and amplitude of HOMO and LUMO, we are able to predict good connections for coherent electron transport in molecular systems. The validity of our orbital rule was experimentally confirmed by conductance measurements of some naphthalene dithiol derivatives with nanofabricated mechanically controllable break junctions.[41]

The orbital rule for electron transport can be viewed as an orbital-interference effect in electron transport because the essence of the rule is the quantum interference between HOMO and LUMO. From 1988 to the early 2000s, the quantum interference effect in molecular junctions was investigated mainly in the concept of path-interference effect by using ring-shaped molecules while the quantum interference was confirmed also in nonring-shaped molecules in which electron pathways cannot be identified. We found the simple concept of the HOMO-LUMO interference when analyzing the quantum transport

through nanographite molecules.[30-32] The orbital rule has been revisited as a quantum interference effect on single molecular conductance.[42-57] Since the quantum interference effect leads to a significant difference in current (i.e., the constructive/destructive interference) through a molecular junction, the presence of the quantum interference effect was firstly elucidated from the viewpoint of current magnitude.[41,58-61] In addition to the indirect observation of the quantum interference effect, a direct observation based on differential conductance was recently performed.[62] Figure 1 clearly exhibits a recent hot situation on the research of the quantum interference effects in molecular junctions.

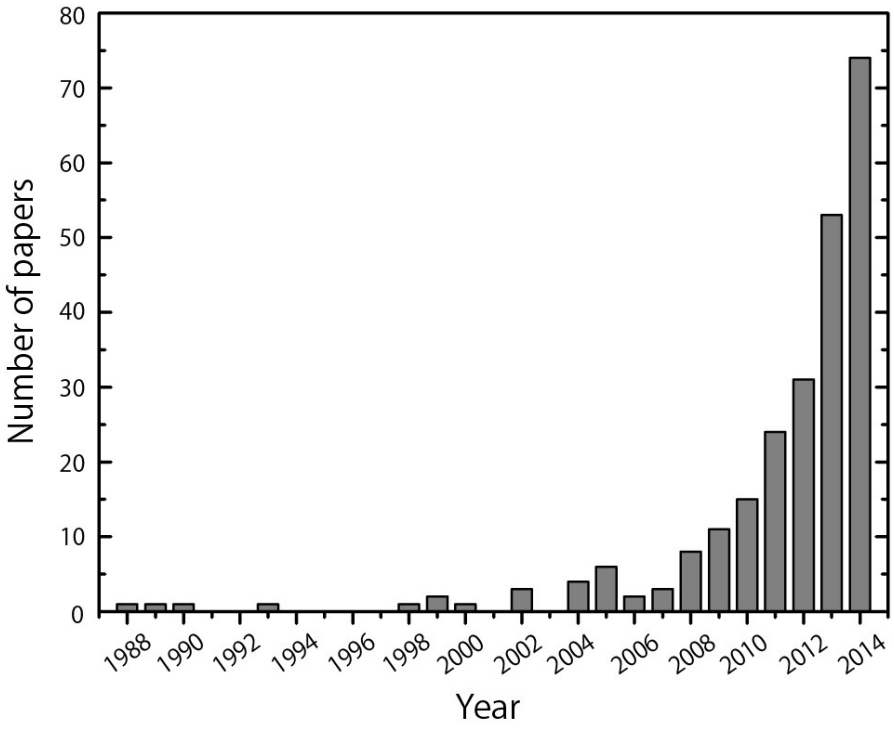

Figure 1. The number of papers for quantum interference effects on electron transport in molecular junctions.

The purpose of this perspective is to explain our way of understanding electron

transport phenomena in molecules and its application to developing conductance-decay free units on the basis of the qualitative orbital thinking. The analysis based on special attention to orbital phase with respect to the physical phenomena is in line with the frontier orbital theory[63] and the Woodward–Hoffmann rules[64] for chemical reactions. It is notable that our orbital thinking derives from Green's function theory while the basis of the chemical reaction theories is on second-order perturbation theory.

Orbital rule of molecular conductance

We have developed an orbital rule for electron transport properties of single molecules from the analysis of Green's function with the simple Hückel method in terms of the orbital concept.[30-33] The orbital rule provides a powerful tool to predict good connection routes through a single molecule. The necessary preconditions for the application of the orbital rule can be summarized as follows: (a) the coupling between a molecule and electrodes is weak, (b) there is electron–hole symmetry or pairing theorem[65] in orbital energies and MO expansion coefficients and (c) the Fermi level is located in the midgap of HOMO and LUMO. These assumptions are reasonable in metal-molecule-metal junctions that consist of dithiol derivatives of π-conjugated systems sandwiched between gold electrodes. According to Landauer's model, the conductance of a metal-molecule-metal junction in the limit of zero temperature and zero bias voltage is written as follows:[18]

$$g = \frac{2e^2}{h} T(E_F) \quad (1)$$

where e is the magnitude of the charge on electron, h is the Planck constant, T is the transmission probability of electron and E_F is the Fermi energy of electrodes. We can calculate the transmission probability for a metal-molecule-metal junction using the retarded/advanced Green's function $G^{R/A}$ of a molecule and the local density of states ρ of metal electrodes as follows:[7,66]

$$T_{rs}(E) = \frac{(2\pi t_c^2)^2}{2} G_{sr}^{A}(E) G_{rs}^{R}(E) \rho^2(E), \tag{2}$$

where indices r and s are the sites connected with metal electrodes, and t_c is the resonance integral (i.e., a hopping integral in physicists' notation) between site r or s and metal electrodes. Using the unperturbed Green's function (i.e., zeroth Green's function) $G_{rs}^{(0)R/A}$ of the molecule and Green's function of electrodes g_{ele}, the Green's function of the molecule in the junction is written as

$$G_{rs}^{R/A} = \frac{G_{rs}^{(0)R/A}}{(1 - t_c^2 G_{ss}^{(0)R/A} g_{ele})(1 - t_c^2 G_{rr}^{(0)R/A} g_{ele}) - t_c^4 G_{rs}^{(0)R/A} G_{sr}^{(0)R/A} g_{ele}^2} \equiv \frac{G_{rs}^{(0)R/A}}{D}. \tag{3}$$

In a weak coupling condition between the molecule and electrodes, the normalization factor D in eqn. (3) is close to one,[66,67] and thereby the zeroth Green's function plays an essential role in the calculation of electron transmission. At the Fermi energy the matrix elements of the zeroth Green's function, $G_{rs}^{(0)R/A}$, which describes the propagation of tunneling electron from site r to site s through the orbitals in the molecular part, can be written as follows:[68]

$$G_{rs}^{(0)\mathrm{R/A}}(E_\mathrm{F}) = \sum_k \frac{C_{rk} C_{sk}^*}{E_\mathrm{F} - \varepsilon_k \pm i\eta} \tag{4}$$

where C_{rk} is the kth MO coefficient at site r, the asterisk on the MO coefficient indicates complex conjugate, ε_k is the kth MO energy and η is an infinitesimal number determined by a relationship between the local density of states and the imaginary part of Green's function.[30,31] Eqn. (4) tells us about an important correlation between the MOs and Green's function and how to use it. The role of the HOMO and LUMO is significant in the zeroth Green's function because the denominators of the two orbitals are small in comparison with those of other MOs in eqn. (4) when we assume the Fermi energy of electrodes to lie between the HOMO and LUMO. The contributions from the HOMO and LUMO in eqn. (4) are written as follows:

$$\frac{C_{r\mathrm{HOMO}} C_{s\mathrm{HOMO}}^*}{E_\mathrm{F} - \varepsilon_\mathrm{HOMO}} + \frac{C_{r\mathrm{LUMO}} C_{s\mathrm{LUMO}}^*}{E_\mathrm{F} - \varepsilon_\mathrm{LUMO}} \equiv G_{rs}^{(0:\mathrm{HOMO,LUMO})}(E_\mathrm{F}) \tag{5}$$

In eqn. (5), we omitted the infinitesimal number η for simplicity. Considering the reversed signs in the two denominators in eqn. (5), we can develop a simple orbital rule useful for chemical understanding. To obtain effective electron transport through a single molecule, (1) two atoms in which the sign of the product of the MO expansion coefficients in the HOMO ($C_{r\mathrm{HOMO}}C^*_{s\mathrm{HOMO}}$) is different from that in the LUMO ($C_{r\mathrm{LUMO}}C^*_{s\mathrm{LUMO}}$) should be connected with electrodes and (2) two atoms in which the orbital amplitudes of the HOMO and LUMO are large should be connected with electrodes.[30,33,39,69] The importance of the orbital amplitudes of HOMO and LUMO was confirmed also in charge injection probabilities of molecular-based solar cells.[70]

Electron transport in benzene molecular junctions

Having described essential features of the orbital rule, let us next explain the electron transport properties of the benzene molecule connected in different ways with two one-dimensional electrodes as an example. We adopted the gold-benzene-gold junctions shown in Fig. 2 to look at the orbital rule because the ring-shaped molecule was firstly introduced by Sautet and Joachim,[71] in which the electron transmission through benzene was discussed in terms of quantum interference effects while the electron transmission at the Fermi level (i.e., conductance) was not discussed.

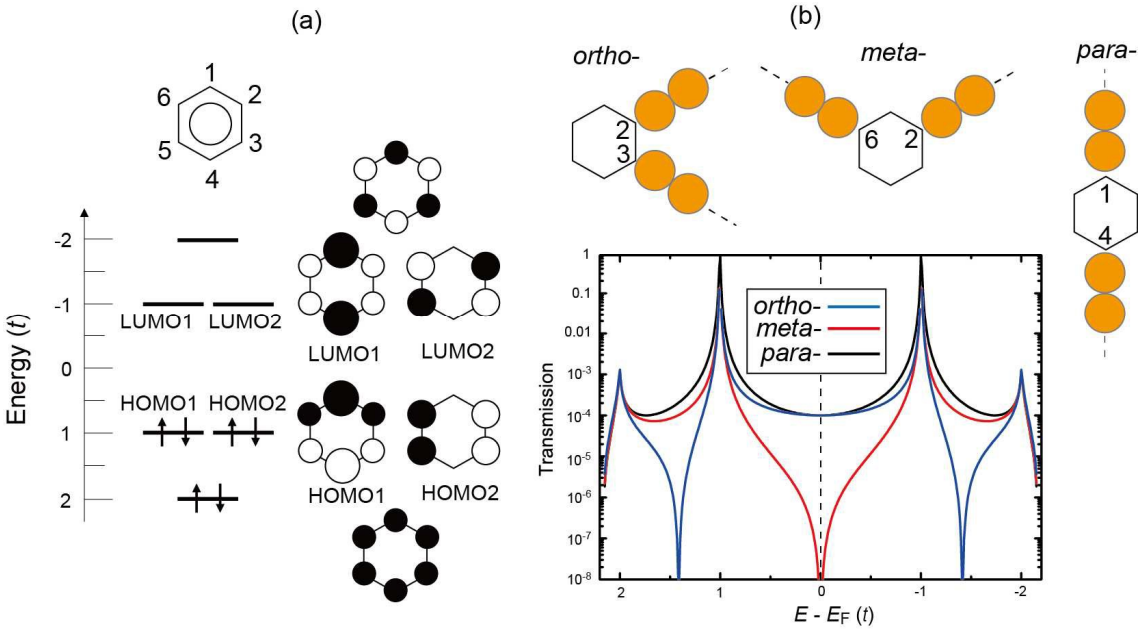

Figure 2. Electron transport properties of benzene molecular junctions. (a) Orbital energies and orbital coefficients of the six π MOs of benzene. (b) Three configurations of the benzene junctions with one-dimensional electrodes (dark yellow), and calculated transmission functions of the three configurations.

The π-MOs of benzene are shown in Fig. 2(a), in which the resonance integral is defined as *t*. The zeroth Green's function of benzene is calculated with the MO energies and MO expansion coefficients according to eqn. (4) and then transmission function is calculated with eqns. (2) and (3). To characterize the transmission function in terms of the MOs of benzene, we use the zeroth Green's function based only on the frontier orbitals of benzene (i.e., eqn. (5)). Since the frontier π-orbitals of benzene are degenerated as shown in Fig. 2, the zeroth Green's function in terms only of frontier orbitals has to be slightly changed from $G^{(0:\text{HOMO, LUMO})}$ in eqn. (5) to the following expression as;

$$\frac{C_{r\text{HOMO1}}C^{*}_{s\text{HOMO1}}}{E_{\text{F}}-\varepsilon_{\text{HOMO1}}\pm i\eta}+\frac{C_{r\text{HOMO2}}C^{*}_{s\text{HOMO2}}}{E_{\text{F}}-\varepsilon_{\text{HOMO2}}\pm i\eta}+\frac{C_{r\text{LUMO1}}C^{*}_{s\text{LUMO1}}}{E_{\text{F}}-\varepsilon_{\text{LUMO1}}\pm i\eta}+\frac{C_{r\text{LUMO2}}C^{*}_{s\text{LUMO2}}}{E_{\text{F}}-\varepsilon_{\text{LUMO2}}\pm i\eta}$$
$$\equiv G_{rs}^{(0:\text{HOMO1,HOMO2,LUMO1,LUMO2})}(E_{\text{F}}), \qquad (6)$$

where HOMO1 and HOMO2 are degenerated and LUMO1 and LUMO2 are also degenerated. In general, the expression based on the four frontier orbitals requires a little more careful analysis to derive the orbital rules for electron transport. However, as described in the next section, the zeroth Green's function based only on "two" frontier orbitals is enough to understand the electron transport in the benzene molecular junctions with one-dimensional electrodes.

In the benzene molecular junctions, three configurations, *ortho*-, *meta*- and *para*-junctions shown in Fig. 2(b) are possible. The calculated transmission function in Fig. 2(b) shows the four peaks at $2t$, t, $-t$ and $-2t$ in energy, which respectively correspond to the transmission peaks originated from the π-orbitals at $2t$, t, $-t$ and $-2t$. At first, let us explain the electron transport properties of the *para*-junction. In this junction, the carbon atoms available

for the connection with the one-dimensional electrodes are fixed to be carbons 1 and 4 because of the symmetry restriction of the *para*-junction. If we use carbons 3 and 6 (or 2 and 5) for the connection sites, the rotational and mirror symmetries in the *para*-junction structure are broken in the MO representation, and thus the connection points are allowed only for carbons 1 and 4. Since the connection points in the *para*-junction are 1 and 4, the contributions from HOMO2 and LUMO2 in the zeroth Green's function are zero. Therefore the important frontier orbitals in the *para*-junction of benzene are HOMO1 and LUMO1, which enables us to use the orbital rules obtained with two frontier orbitals. According to the orbital phases in Fig. 2(a), the sign of $C_{1\,\mathrm{HOMO1}}C_{4\,\mathrm{HOMO1}}$ is negative, and that of $C_{1\,\mathrm{LUMO1}}C_{4\,\mathrm{LUMO1}}$ is positive. This is a case for the constructive interference between the frontier orbitals, and therefore we obtained a non-zero transmission value at the Fermi energy in the *para*-junction. In addition, the orbital phases of HOMO1 and the lowest π-orbital at $2t$ successfully explain why the transmission values in the energy range from $2t$ to t also show non-zero values; the constructive relationship between the two π-orbitals is confirmed because the connecting carbons are 1 and 4. In the same way, the non-zero transmission values in the range from $-t$ to $-2t$ are understood from the orbital phases of LUMO1 and the highest π-orbital at $-2t$.

Let us next consider the *meta*-junction, in which the connections are allowed for carbons 2 and 6 (or 3 and 5) because of the symmetry restriction (i.e., mirror symmetry) in the *meta*-junction structure. If we use other combinations (e.g., carbons 1 and 3), the rotational and mirror symmetries in the *meta*-junction structure are broken in the MO representation. Thus, in contrast to the *para*-junction, the connecting carbon atoms have non-zero orbital amplitudes in the four frontier orbitals, which requires the four-orbital based zeroth Green's

function in eqn. (6). However, the additive property in the Green's function means that MOs with large amplitudes have more significant contributions in the Green's function than those with smaller ones. In the *meta*-junction, the amplitudes at carbons 2 and 6 in HOMO2 (LUMO2) are larger than those in HOMO1 (LUMO1) (see Fig. 2(a)), and thus the important two frontier orbitals in the *meta*-junction are HOMO2 and LUMO2. The sign of $C_{2\,\mathrm{HOMO2}}C_{6\,\mathrm{HOMO2}}$ is negative, and that of $C_{2\,\mathrm{LUMO2}}C_{6\,\mathrm{LUMO2}}$ is also negative. Thus, this is the destructive interference between the frontier orbitals in the *meta*-junction. Consequently, the zero transmission at the Fermi energy appears in the *meta*-junction. On the other hand, when we focus our attention to the energy range from $2t$ to t ($-t$ to $-2t$), the important two orbitals are HOMO2 and the lowest π-orbital at $2t$ (LUMO2 and the highest π-orbital at $-2t$), and we can easily confirm a constructive relationship in the *meta*-junction, corresponding to the non-zero transmission in the energy range from $2t$ to t ($-t$ to $-2t$).

In the *ortho*-junction, carbons 2 and 3 (or 5 and 6) are possible atoms for the connections from the symmetry conditions in the *ortho*-junction structure, and HOMO2 and LUMO2 are again the important frontier orbitals. The sign of $C_{2\,\mathrm{HOMO2}}\,C_{3\,\mathrm{HOMO2}}$ is positive and that of $C_{2\,\mathrm{LUMO2}}\,C_{3\,\mathrm{LUMO2}}$ is negative, indicating a constructive interference and thereby the non-zero transmission appears at the Fermi energy in the *ortho*-junction. The destructive interference at the energy range from $2t$ to t ($-t$ to $-2t$) is also successfully explained from HOMO2 and the lowest π-orbital at $2t$ (LUMO2 and the highest π-orbital at $-2t$). In this way, the orbital rule for electron transport is quite robust for an easy prediction of transport properties in π-conjugated molecular junctions. Examples for other molecular junctions in which the orbital rule is applied to understand the transport properties are found in our previous studies.[33,35]

Electron transport in one-dimensional π-conjugated molecular junctions

In this perspective let us focus on the exponential decay of conductance as a function of wire length to design conductance-decay free junctions,[2,10,32,72] and we introduce one-dimensional chains as π-molecules sandwiched between electrodes. Figure 3 shows the molecular orbitals of hexatriene C_6H_8 with bond alternation. Looking at the HOMO and LUMO in terms of the orbital rule for electron transport, carbons 1 and 6 are found to be good connection sites with electrodes for large conductance. Although carbons 3 and 4 are also effective for large conductance, such a combination is not appropriate for the investigation of long molecular units for electron transport because we cannot effectively extend the electrode-electrode distances in such a connection. We thus select the two edge carbons of one-dimensional chains for the connecting points with electrodes. Since the overlap integral between carbons are neglected in the Hückel method, there is electron–hole symmetry or pairing theorem with respect to the MO energies and MO expansion coefficients. The relationship for good conductance thus holds true also in a pair of HOMO – 1 and LUMO + 1, a pair of HOMO – 2 and LUMO + 2, due to the electron–hole symmetry at the Hückel level of theory.[39,65] A calculated transmission function of the hexatriene junction in the edge connection with electrodes is shown in Fig. 3(b).

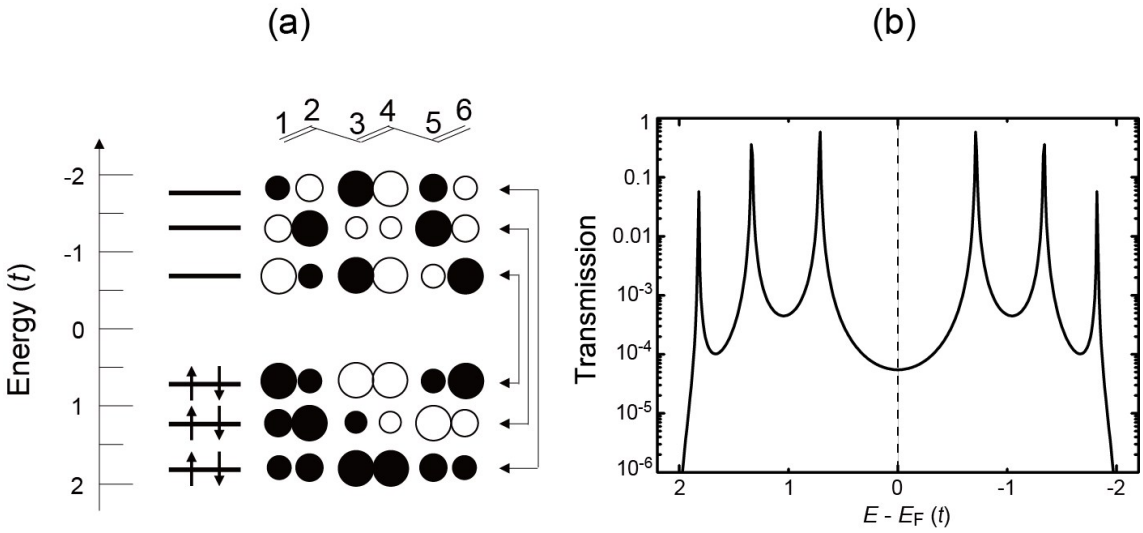

Figure 3. (a) The six π MOs and (b) a calculated transmission function of hexatriene with bond alternation. The transfer integrals t between adjacent carbon atoms are 1.2 t (double bond) and 0.8 t (single bond).

When we focus on long molecular units for electron transport, the wire length dependence on conductance is an important property to be investigated. Figure 4 shows calculated transmission functions for the C_nH_{n+2} (n = 6, 8, 10, 12 and 14) junctions with one-dimensional electrodes, and it indicates that the conductance is decreased with an increase in chain length. According to the Green's function expression for conductance, the conductance is proportional to the square of orbital amplitudes and inversely proportional to the energy gap between HOMO (or LUMO) and Fermi energy. Despite the fact that the HOMO and LUMO levels becomes energetically closer to the Fermi energy in longer chains (Fig. 4 and Table I), the conductance decreases as a function of wire length. Thus, the orbital amplitudes have significant contributions to the conductance decrease. When frontier orbitals are delocalized in a wider/longer region, the amplitudes of the frontier orbitals at the edges of the wire are decreased with an increase in chain length. In the present carbon chains, Table I

clearly indicates a rapid decrease of orbital amplitudes in longer chains.

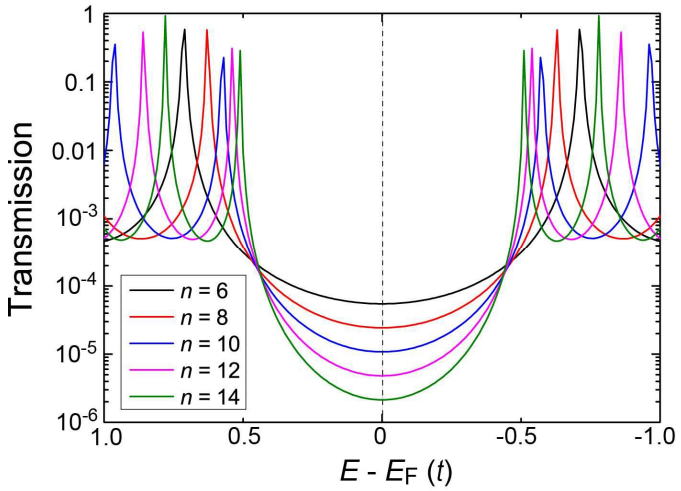

Figure 4. Calculated transmission functions of bond alternated C_nH_{n+2} (n = 6, 8, 10, 12 and 14) junctions. The transfer integrals t between adjacent carbon atoms are 1.2 t (double bond) and 0.8 t (single bond).

(Table I here)

To characterize the conductance decrease as a function of molecular length, the exponential expression for conductance is useful as $G = G_0 \exp[-\beta l]$, where G_0, l and β are respectively the contact conductance, the molecular length and the decay factor per unit length.[2,10,32,72] Using the calculated conductance (i.e., the transmission function at the Fermi energy) in the one-dimensional carbon chains, we obtained 0.29 ($Å^{-1}$) of β, which is a typical value for β in conjugated chains. The β values for other systems were found in many theoretical/experimental studies.[32,41,72-74]

Let us next consider how conductive molecular junctions with a small decay factor should be designed. Green's function in eqn. (3) is again quite helpful for looking at the

design concept. Since we have already confirmed that the amplitudes of frontier orbitals are a dominant factor for conductance variations in terms of wire length, holding large orbital amplitudes at the molecular edges in longer chains will be a necessary condition. To realize the condition, we consider artificial one-dimensional chains in which the atomic orbital (AO) energies (i.e., on-site energy in physicists' notation) in the middle –C=C– units are shifted from the original value of ε_0 (0.0 t) to ε_z (Fig. 5(a)). In the AO-shifted chain, the interaction between the left-/right-side edge and middle units becomes smaller than that in the original chain, leading to the suppression of orbital delocalization between the edge and middle units, and thereby the orbitals at the edge unit are more localized than that in the original chain. Once the orbital is localized at the edges, large orbital amplitudes at the edge units will be kept even in longer chains because of small interactions between the edge and middle units.

Figure 5(b) shows calculated charge distributions in the HOMO of $C_{14}H_{16}$ for the AO shift with $0.0|t|$, $–0.5|t|$ and $–1.0|t|$. The larger the magnitude of the AO-shift in the middle units (i.e., sites 3 to 12) becomes, the more prominent the electron localization at the edge units (i.e., sites 1, 2, 13 and 14) becomes. Since the resonance integral t in carbon systems is about –2 eV, the AOs with the downward shift of $–1.0|t|$ correspond to N atoms. The AO energy of carbon 2p is –11.4 eV and that of nitrogen 2p is –13.4 eV. Figure 5(c) shows a calculated transmission function using the AO shift of $–1.0|t|$ and indicates the clear enhancement of transmission function at the Fermi energy compared with the original carbon chain, $C_{14}H_{16}$. In addition, we also obtained a smaller decay factor of 0.17($Å^{-1}$) in a series of AO-shifted chains (Fig. 5(d)) because the orbital amplitudes of the localized orbitals at the edges are larger and less sensitive to the molecular length than that in the original chain (See Table II). In particular, the contribution to the conductance from HOMO (i.e.,

(C_{HOMO})^2/ ε_{HOMO}) is surprisingly increased with an increase in the chain length of AO-shifted chains, which is not observed in the original carbon chains. The quantities (C_i)^2/ε_i except for the edge-localized frontier orbitals are naturally decreased with an increase in chain length (Table I). Consequently, the prominent contributions from the edge-localized frontier orbitals on conductance result in a smaller decay factor of conductance than that of the original chain. Along this concept, if only the edge-localized frontier orbitals contribute to conductance, we can expect an eccentric molecular junction that shows a conductance "increase" with an increase in chain length. In fact, such a conductance increase (i.e., the reverse exponential law of conductance decay)[32] was already proposed in nano graphite molecular series with zigzag edges for contact points. Since the zigzag edge state tends to appear in the vicinity of the Fermi energy, the contributions from the edge localized frontier orbitals (i.e., zigzag edge states in the nano graphite) are totally emphasized, leading to the conductance increase with an increase in wire length. These design concepts for small decay factors and reverse exponential law of conductance decay are obtained on the basis of qualitative orbital thinking.

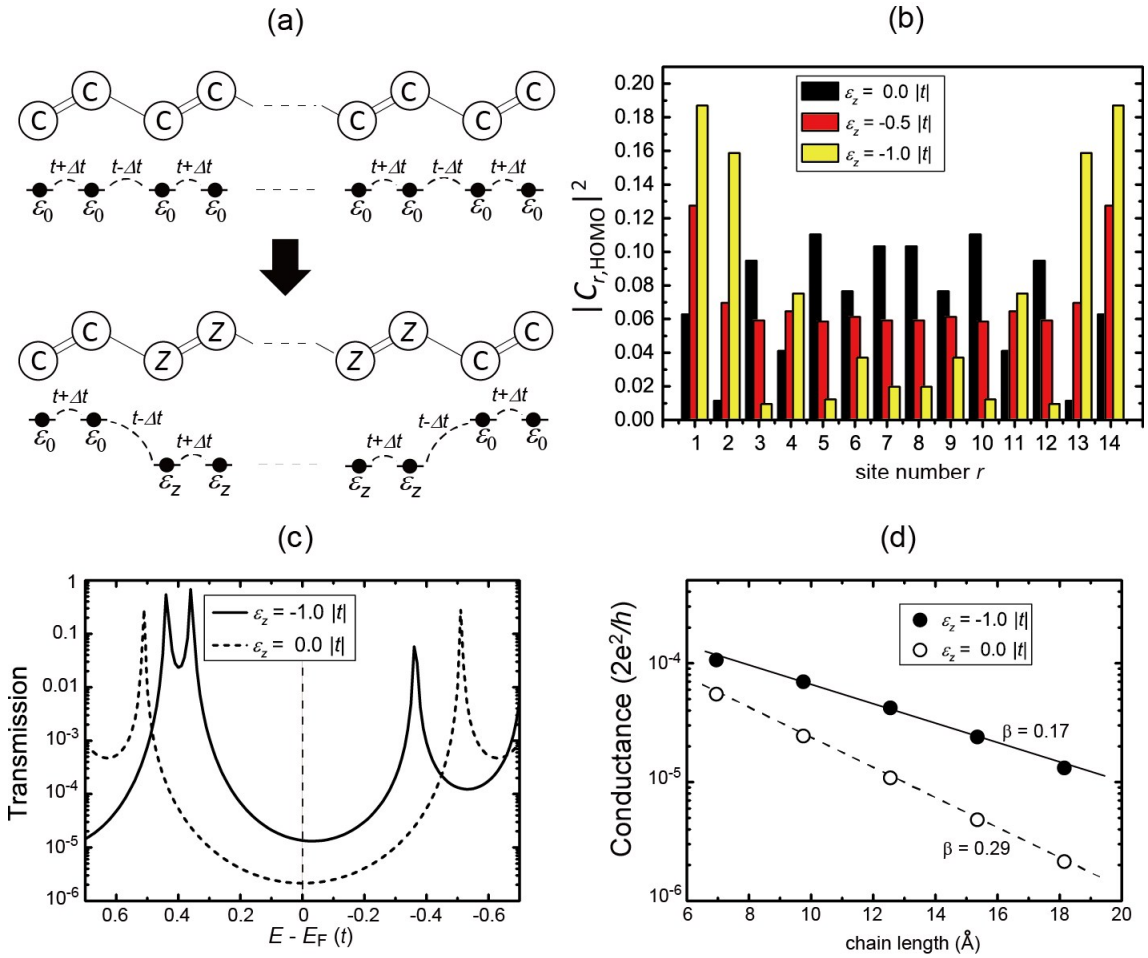

Figure 5. Small decay factor of conductance in one-dimensional chains. (a) Carbon chains with and without atomic orbital shifts at the middle units. (b) Charge distributions in HOMOs, $|C_{r\mathrm{HOMO}}|^2$, with the atomic orbital shifts of 0.0, -0.5$|t|$, and -1.0$|t|$. (c) Calculated transmission functions of $C_{14}H_{16}$ junction with and without atomic orbital shifts. (d) Calculated conductance (transmission function at the Fermi energy) as a function of chain length and the decay factors.

(Table II here)

Although the orbital localization at the edge unit is required for a small decay factor, the "perfect" localization at the edge is rather problematic because electron transport requires

molecular orbitals that are expanded over molecular unit.[75] That is, the key concept for the molecular junction with a small decay factor is designing the edge and middle units so as to make frontier orbitals moderately localized at the edge units without the "perfect" break down of orbital delocalization between the edge and middle units.

Although the concept for the conductance-decay free junctions is clearly identified, such a molecular junction, especially for the nano graphite with zigzag-edge showing the conductance increase, has not been realized in experimental studies because of the difficulty in the precise control of zigzag structure due to the energetical destabilization and the contact with electrodes at the zigzag edges. However, we can find good examples in recent experimental studies on π-stacked molecular junctions, in which the electron transport property is in line with the concept for the conductance-decay free junction.[76-78]

Electron transport in π-stacked junctions and small decay factors of conductance

To sandwich a fixed number of π-stacked molecules (molecule **4** in Fig. 6(a)) between electrodes, cage-shaped super molecules that have a fixed nano space in its inside (molecules **1**, **2** and **3** in Fig. 6(a)) are adopted to construct π-stacked molecular junctions. The cage-shaped super molecules are composed of two π-conjugated molecular panels (molecule **6** in Fig. 6(a)), three pillars of molecule (molecule **7a**/**7b**/**7c** in Fig. 6(a)) and Pd-complexes (molecule **5** in Fig. 6(a)) at the corners of the super molecules. A recent experimental study based on the STM break junction method reveals that electron tunneling is observed when π-conjugated molecules (molecule **4**) is included in the cages (i.e., **1**•(**4**)$_2$, **2**•(**4**)$_3$ and **3**•(**4**)$_4$ in Fig. 6(a)), whereas no tunneling in the empty cages (i.e., **1**, **2** and **3** in Fig. 6(a)).[76] Therefore the π-stacked molecular junction can be realized in the configuration shown

in Fig. 6(b), and thereby the computational models for the π-stacked junctions are constructed in order to include important building blocks for the π-stacked junction (i.e., two π-conjugated molecular panels (**6**), π-molecules (**4**) and electrodes, which are directly connected to the π-conjugated molecular panels in both sides (Fig. 6(c)).

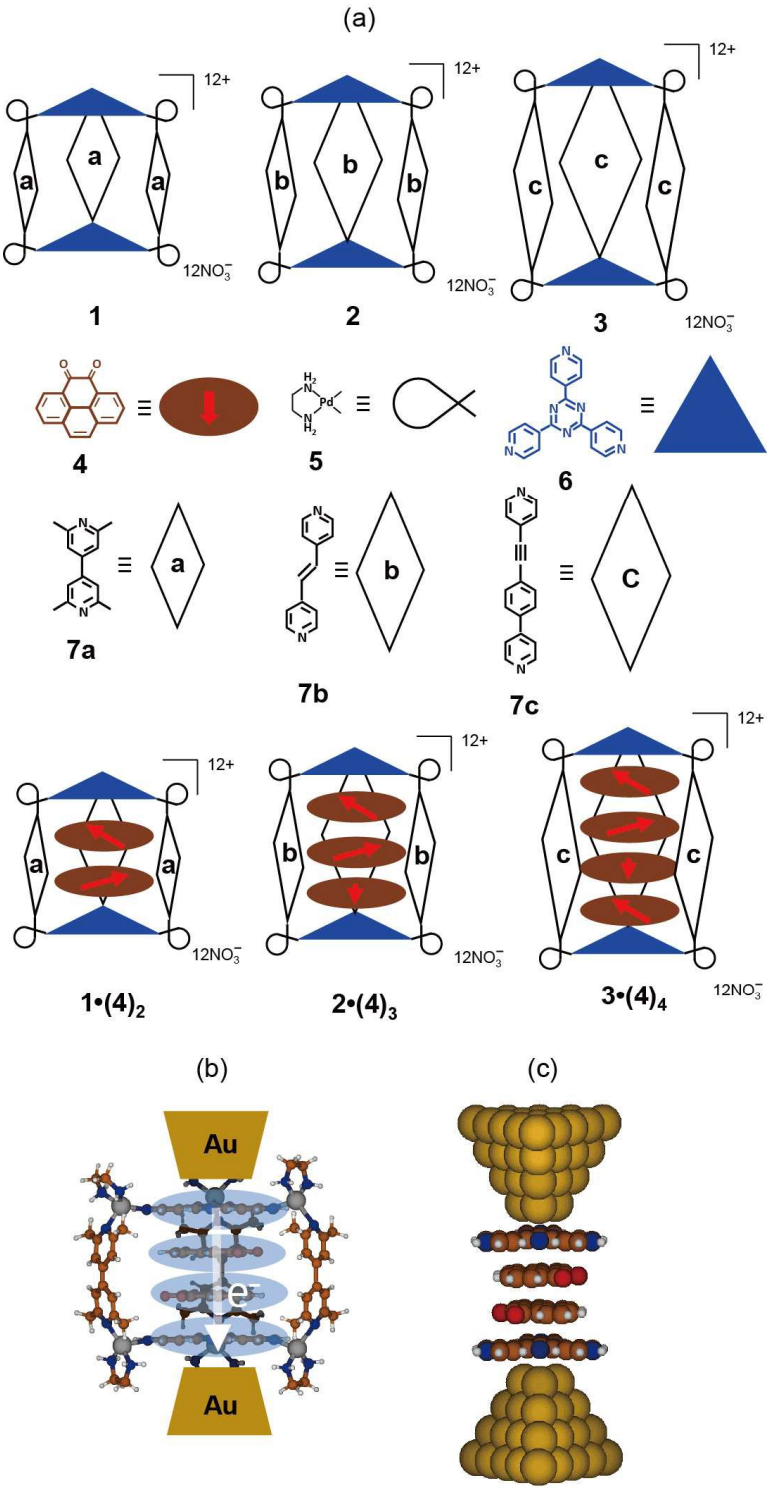

Figure 6. π-stacked molecular junctions. (a) Molecular units constituting π-stacked super molecules. (b) Expected junction configuration **1**•(**4**)$_2$ for electron transport through π-stacking and (c) the computational model **6**•(**4**)$_2$•**6** for conductance calculation.

The NEGF method is adopted again for the conductance calculations, as already demonstrated in the previous sections for the benzene and simple carbon chains. Although the Hückel type Hamiltonian is convenient to figure out the roles of electronic states of molecules on electron tunneling, the simple approximation for electronic structure calculations is insufficient for quantitative calculations of conductance in comparison with experimental results. Thus, a standard approach in this research field is the NEGF calculations based on DFT, which is one of the most successful approximations for the calculations of molecular conductance. However, even in the NEGF-DFT calculations, underestimated HOMO-LUMO gaps in DFT would cause an overestimation of conductance of molecular junctions because the frontier orbital levels are much closer in energy to the Fermi level than those in realistic (i.e., experimental) conditions. Therefore advanced approaches based on configuration interaction,[79,80] self-interaction correction[81,82] and GW approximation[83,84] are recently proposed for quantitative conductance calculations although the computational costs in these approaches are huge. To overcome those difficulties in the quantitative conductance calculations, we developed an NEGF method based on hybrid-DFT in cluster approach[85,86] (Fig. 7(a)). The hybrid-DFT improves the problems of underestimation of gaps in DFT, and cluster approach enables us to carry out simple calculations of conductance like electronic structure calculations for molecules. Since details of the approach are written in our original study,[85] we simply explain the essence of the approach as follows.

1) The cluster model for a molecular junction is composed of a left metal cluster, a sandwiched molecule and a right metal cluster.

2) The sandwiched molecule and some metal atoms in both clusters are defined as an extended molecule.
3) Metal cluster atoms except for the metal atoms included in the extended molecule are recognized as electrode clusters, and the density of states of the metal clusters are broadened to obtain Green's functions of metal clusters (i.e., metal electrodes).
4) Broadening parameters for the metal clusters are chosen so as to show a reasonable conductance in a reference system (e.g., $2e^2/h$ in a one-dimensional gold chain).
5) The size of metal cluster is determined to hold the condition that the calculated conductance is almost insensitive to the cluster size.

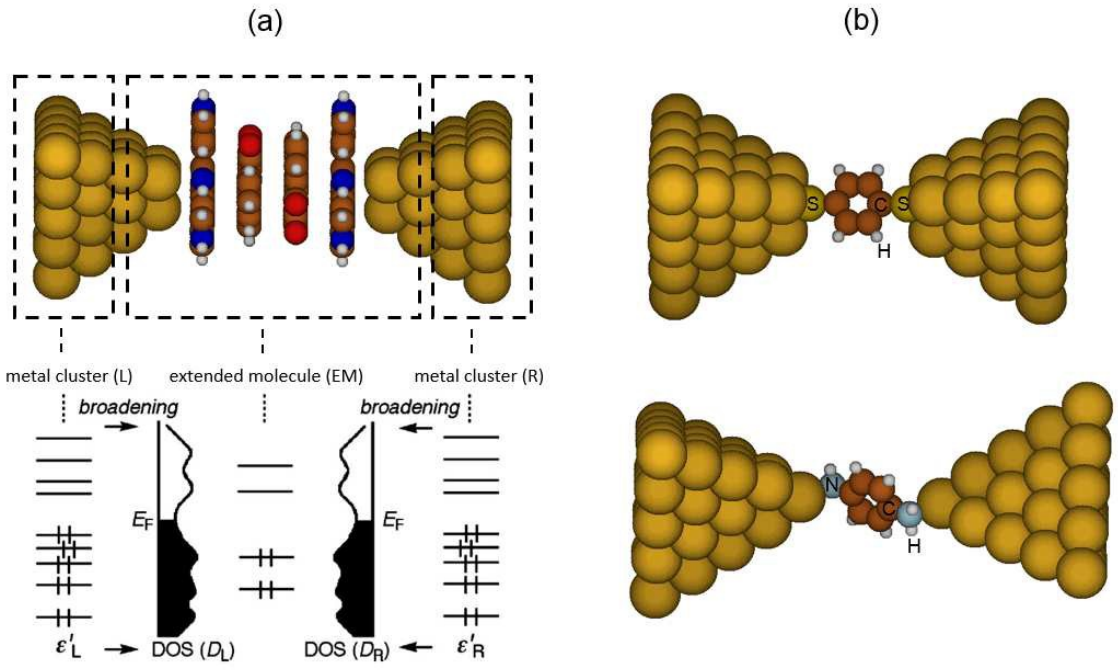

Figure 7. Computational models in the cluster approach based on hybrid-DFT for quantitative conductance calculations. (a) Theoretical concept for conductance calculations in the cluster approach. (b) Cluster models for BDT (top) and BDA (bottom) junctions.

Now that we explained the computational framework in the cluster approach, we introduce some examples of benzene-dithiol (BDT)[87-89] and benzene-diamine (BDA)[90,91] molecular junctions as benchmark systems. The cluster models of Au_{34}-BDT-Au_{34} and Au_{35}-BDA-Au_{35} shown in Fig. 7(b) were used for conductance calculations; the extended molecules for both systems are respectively Au_9-BDT-Au_9 and Au_{10}-BDA-Au_{10}. As for the adsorption site of molecules on metal, the most probable adsorption sites (i.e., the hollow site for BDT and on-top site for BDA) were adopted. In the present calculations with the cluster approach, the B3LYP[92,93]/Lanl2DZ[94-96] level of hybrid DFT was adopted for conductance calculations. Table III lists calculated and observed conductance for the BDT and BDA junctions together with computational results with standard NEGF-DFT[22,97,98] using the Perdew-Burke-Ernzerhof (PBE)[99] functional in the generalized gradient approximation (GGA) and DZP basis sets. The calculated conductance with NEGF-DFT shows about a one-order larger value than those of experimental data, which is caused by the underestimation of the HOMO-LUMO gaps of the sandwiched molecules. On the other hand, NEGF-hybrid DFT calculations in the cluster approach show quantitatively comparable conductance to experimental data. The quantitative good correspondence between the calculated conductance with NEGF-hybrid DFT and experimental one is found also in other molecular junctions,[85] and thus NEGF-hybrid DFT is more suitable for quantitative calculations of conductance of molecular junctions than the standard NEGF-DFT method.

(Table III here)

We adopted the NEGF-hybrid DFT method in the conductance calculations also for the π-stacked molecular junctions. Since the π-panel molecule is directly linked with electrode as π-bonding, we used direct π-contact in the junctions as shown in Fig. 7(a). The metal cluster size for both sides is the same in the BDT junction, Au_{34} for each metal cluster.

According to the experimental studies on π-stacked junctions,[76] the numbers of π-conjugated molecules inserted in the nano-space are 2, 3 and 4 by controlling the length of pillar molecule of the cage (molecules **7a**, **7b** and **7c**), and thus we adopted the junction models as Au_{34}-**6**(**4**)$_n$**6**-Au_{34}, where *n* is the number of stacking molecules **4** between the two panel molecules. The level of B3LYP/Lanl2DZ in hybrid DFT was used again for the π-stacked junctions. Calculated transmission functions of the π-stacked junctions are shown in Fig. 8(a) together with the computational models (Fig. 8(b)), and the conductance values as a function of stacking length are shown in Fig. 8(c). Using the exponential expression of conductance, we obtained a decay factor β of 0.097 $Å^{-1}$, which is quite a small value compared with typical molecular junctions, and is almost identical to an experimentally determined value of 0.1 $Å^{-1}$.[76]

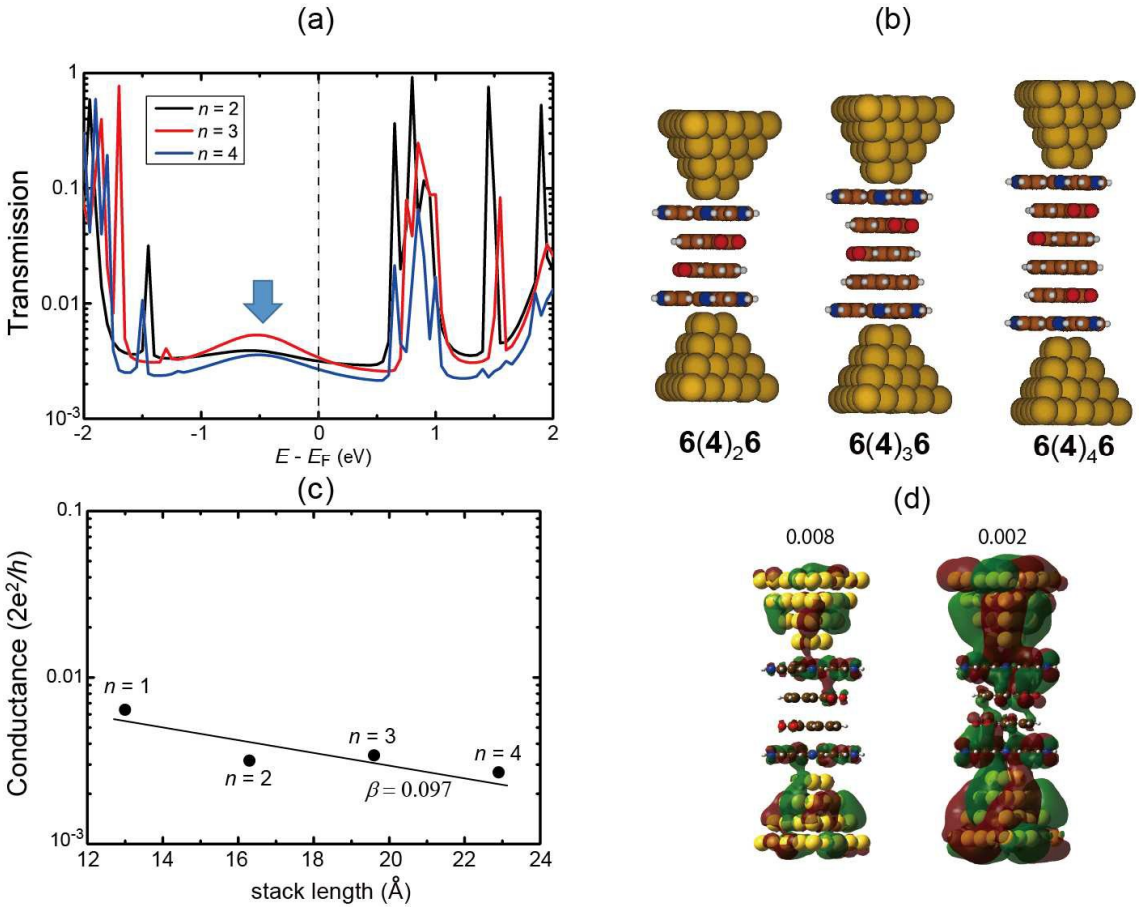

Figure 8. Electron transport of π-stacked molecular junctions. (a) Calculated transmission functions of **6(4)$_2$6**, **6(4)$_3$6** and **6(4)$_4$6** junctions and (b) the computational models for the conductance calculations. (c) Calculated conductance as a function of stacking length. π-stacked junction of **6(4)$_1$6** was also included in the calculation of the decay factor β of conductance. (d) Molecular orbital of **6(4)$_2$6** at 0.5 eV below the Fermi energy (the peak position indicated with the blue arrow in (a)). The numbers are the isosurface values in the unit of e^-/au^3

To elucidate the origin of the small decay factor in the π-stacked junctions, we focus our attention to the broad peaks of the transmission at 0.5 eV below the Fermi energy, which is indicated with an arrow in Fig. 8(a). The transmission values at the Fermi energy has a significant contribution from the broad transmission peaks. Figure 8(d) shows the molecular

orbitals of Au_{34}-**6**(**4**)$_2$**6**-Au_{34} at the peak position; the isosurface values (0.008 and 0.002 e^-/au^3) were used in the orbital drawing. Figure 8(d) indicates that the molecular orbital is totally delocalized over the π-stacking of **6**(**4**)$_2$**6**, and that the orbital amplitudes are relatively concentrated on the edge π-panels **6**. The former is necessary for the electron conduction through the junction, and the latter is required for a small decay factor of electron tunneling, that is, the edge localization. Thus, the conditions for the small decay of conductance is realized in the **6**(**4**)$_n$**6** π-stacked junctions.

Although the small decay of conductance is obtained in the **6**(**4**)$_n$**6** π-stacked junctions, there still be a chance for further enhancement of the conductance value itself. Therefore in order to increase the transmission values, we expect that there is another π-conjugated molecule replacing molecule **4** in **6**(**4**)$_n$**6** stack to enhance the conductance value. The alternative π-conjugated molecule newly introduced in the cage instead of molecule **4** is shown in Fig. 9, together with the model junctions of Au_{34}-**6**(**8**)$_n$**6**-Au_{34}. The π-conjugated molecule **8** includes Au atoms as Au(I) ion,[77] and we thus expect the transport channel inside the π-stacking becomes more conductive.

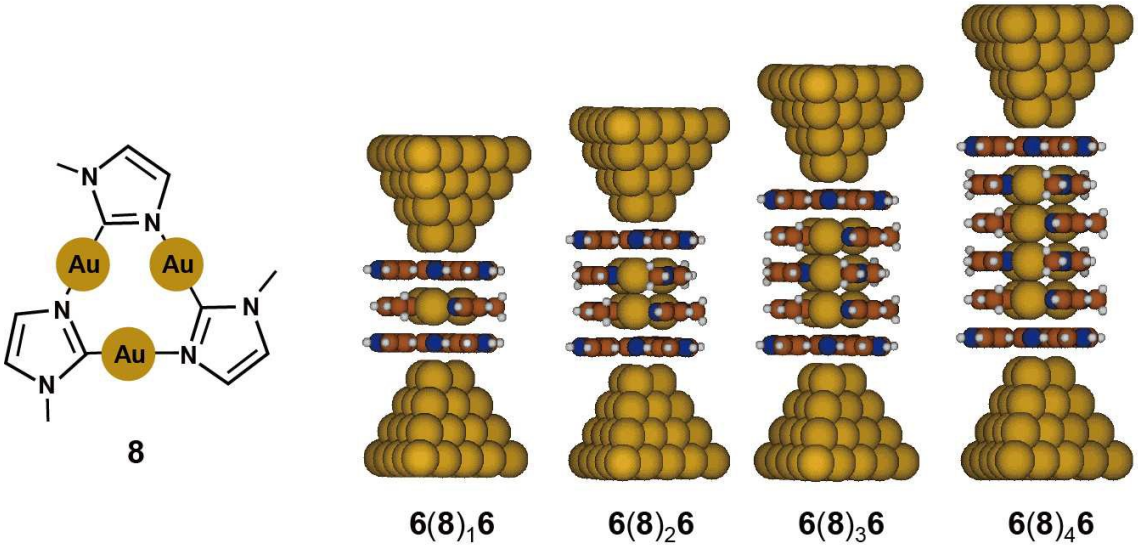

Figure 9. Schematic representation of a π-conjugated molecule including three Au(I) ions and

the computational models for the π-stacked molecular junctions including the $Au(I)_{3n}$ (n = 1, 2, 3 and 4).

A calculated transmission function of **6**(**8**)$_2$**6** is shown in Fig. 10(a), and the enhancement of conductance by about one order from **6**(**4**)$_2$**6** is successfully achieved as expected. Figure 10(b) shows the conductance dependence on the stacking length of **6**(**8**)$_n$**6**, where the decay factor is still quite small. The decay factor in **6**(**8**)$_n$**6** is about two times smaller than that of **6**(**4**)$_n$**6**, and almost identical to the experimentally determined value of 0.05.[77] Therefore the design concept for small decay factor with high transmission is validated by exchanging the middle units. In addition, we recognized that the π-stacked junctions have a significant advantage that the electronic functionality of molecular junctions can be tuned by exchanging the π-conjugated molecules integrated in the cage molecule. Thus, the high tunability of the π-stacked junctions will enables us to fabricate an eccentric π-stacked junction that shows a conductance increase with an increase in stacking length or free from the exponential conductance decrease. In fact, a series of π-stacked junctions successfully shows rectifier responses by selecting appropriate donor and accepter π-stacked molecules in the cage.[78] The possibility of π-stack rectifier was theoretically predicted in 2012 prior to the experimental observation on the basis of the orbital thinking.[100]

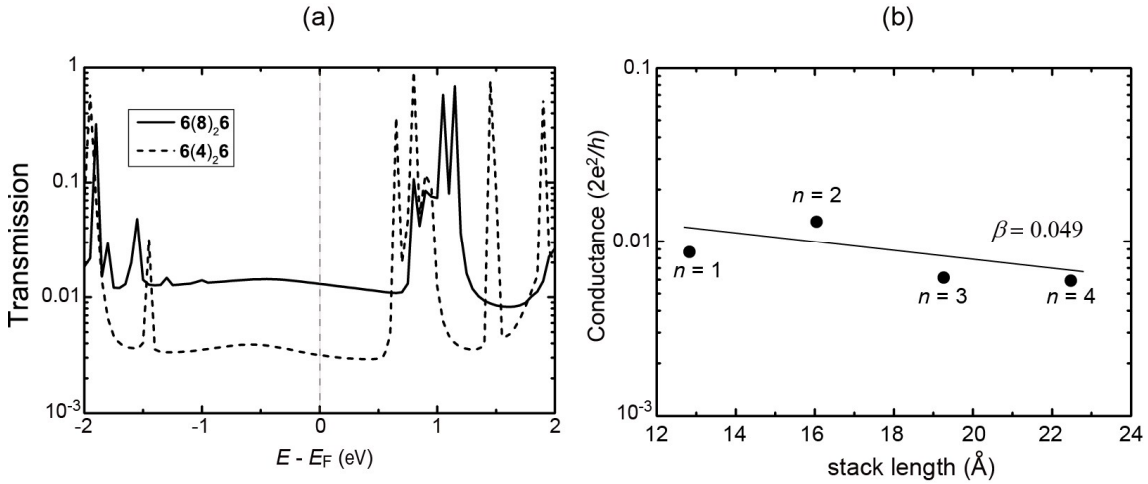

Figure 10. (a) Calculated transmission function of $\mathbf{6(8)_2 6}$ and $\mathbf{6(4)_2 6}$ molecular junctions and (b) calculated conductance as a function of π-stacking length.

Summary

We have presented our way of thinking about electron transport properties of molecules in terms of the orbital concept and explained the orbital rule in detail using the benzene molecular junctions with the *para*-, *meta*- and *ortho*-connections. The validity of the orbital rule for molecular conductance was already confirmed by a collaborative study on single-molecule measurements of naphthalene dithiols,[41] and in turn its power for the design of specific transport properties in molecular junctions is demonstrated in this study. Qualitative predictions based on the orbital concept would help our intuitive understanding of the electron transport phenomena in single-molecular devices and leads to a reasonable design of transport properties. On the basis of this rule, we have discussed linear π-conjugated chains and π-stacked molecular junctions with respect to their small decay factors. In order to design conductance-decay free molecular junctions, moderately edge-localized frontier orbitals are required from the orbital thinking directly derived from Green's function theory. The design concept for conductance-decay free junctions is successfully confirmed in π-stacked

molecular junctions recently fabricated in experimental studies.[76-78] The small decay factor derives from the moderately edge-localized orbitals, as confirmed from DFT calculations. This shows a clear contrast to a long-range electron transfer in a long conjugated chain where electron correlations play an important role.[101]

Acknowledgements

The authors sincerely thank Drs. Masakazu Kondo, Aleksandar Staykov, Daijiro Nozaki, Yuta Tsuji and Xinqian Li for their contributions to the development of the orbital rule. K.Y. is grateful to Professors Tadashi Sugawara, Masateru Taniguchi and Tomoji Kawai for experimental confirmation of the orbital rule using naphthalene dithiol derivatives. T.T. is grateful to Professors Makoto Fujita, Manabu Kiguchi, Takashi Murase and Satoshi Watanabe for collaboration about synthesis, conductance measurements and calculations. This research was supported by Grants-in-Aid for Scientific Research (Nos. 24109014 and 15K13710 to K.Y., Innovative Areas "π-System Figuration: Control of Electron and Structural Dynamism for Innovative Functions" to T.T.) from the Japan Society for the Promotion of Science, the Global COE Project, the Nanotechnology Support Project, the Joint Project of Chemical Synthesis Core Research Institutions from the Ministry of Culture, Sports, Science, and Technology (MEXT) of Japan and CREST of the Japan Science and Technology Cooperation for their support of this work.

Table. I: Calculated orbital energies of HOMO, ε_{HOMO}, orbital coefficients of HOMO at the edge atom, C_{HOMO}, related quantities of HOMO for conductance, $1/\varepsilon_{HOMO}$, $(C_{HOMO})^2$ and $(C_{HOMO})^2/\varepsilon_{HOMO}$ in π-conjugated polyene C_nH_{n+2}.

n	ε_{HOMO}	C_{HOMO}	$1/\varepsilon_{HOMO}$	$(C_{HOMO})^2$	$(C_{HOMO})^2/\varepsilon_{HOMO}$
6	0.71	0.47	1.41	0.22	0.31
8	0.63	0.39	1.59	0.15	0.24
10	0.57	0.33	1.75	0.11	0.19
12	0.54	0.29	1.85	0.08	0.15
14	0.51	0.25	1.96	0.06	0.12

Table. II: Calculated orbital energies of HOMO, ε_{HOMO}, orbital coefficients of HOMO at the edge atom, C_{HOMO}, related quantities of HOMO for conductance, $1/\varepsilon_{HOMO}$, $(C_{HOMO})^2$ and $(C_{HOMO})^2/\varepsilon_{HOMO}$ in π-conjugated polyene C_nH_{n+2} with AO shift.

n	ε_{HOMO}	C_{HOMO}	$1/\varepsilon_{HOMO}$	$(C_{HOMO})^2$	$(C_{HOMO})^2/\varepsilon_{HOMO}$
6	0.55	0.51	1.82	0.26	0.47
8	0.46	0.47	2.17	0.22	0.48
10	0.41	0.45	2.44	0.20	0.49
12	0.38	0.44	2.63	0.19	0.51
14	0.36	0.43	2.78	0.18	0.51

Table. III: Calculated and measured conductance of the BDT and BDA molecular junctions.

Method	BDT	BDA
NEGF-DFT	0.17	0.04
NEGF-Hybrid DFT	0.011	0.008
Experiment	0.011[a]	0.006[b]

[a]Ref. 87

[b]Ref. 90

Notes and References

1 A. Aviram and A. Ratner, *Chem. Phys. Lett.*, 1974, **29**, 277–283.

2 C. Joachim, J. K. Gimzewski and A. Aviram, *Nature*, 2000, **408**, 541–548.

3 R. L. Carroll and C. B. Gorman, *Angew. Chem., Int. Ed.*, 2002, **41**, 4378–4400.

4 A. Nitzan and M. A. Ratner, *Science*, 2003, **300**, 1384–1389.

5 G. Cuniberti, G. Fagas and K. Richter, *Introducing Molecular Electronics*, Springer-Verlag, Berlin, Heidelberg, 2005.

6 R. Landauer, *IBM J. Res. Dev.*, 1957, **1**, 223–231.

7 S. Datta, *Electronic Transport in Mesoscopic Systems*, Cambridge University Press, Cambridge, 1995.

8 V. Mujica, M. Kemp, A. Roitberg and M. Ratner, *J. Chem. Phys.*, 1996, **104**, 7296–7305.

9 M. P. Samanta, W. Tian, S. Datta, J. I. Henderson and C. P. Kubiak, *Phys. Rev. B*, 1996, **53**, R7626–R7629.

10 M. Magoga and C. Joachim, *Phys. Rev. B*, 1997, **56**, 4722–4729.

11 W. Tian, S. Datta, S. Hong, R. Reifenberger, J. I. Henderson and C. P. Kubiak, *J. Chem. Phys.*, 1998, **109**, 2874–2882.

12 M. Olson, Y. Mao, T. Windus, M. Kemp, M. Ratner, M. Léon and V. Mujica, *J. Phys. Chem. B*, 1998, **102**, 941–947.

13 J. C. Cuevas, A. L. Yeyati and A. Martín-Rodero, *Phys. Rev. Lett.*, 1998, **80**, 1066–1069.

14 V. Mujica, A. E. Roitberg and M. Ratner, *J. Chem. Phys.*, 2000, **112**, 6834–6839.

15 H. J. Choi, J. Ihm, S. G. Louie and M. L. Cohen, *Phys. Rev. Lett.*, 2000, **84**, 2917–2920.

16 L. E. Hall, J. R. Reimers, N. S. Hush and K. Silverbrook, *J. Chem. Phys.*, 2000, **112**,

1510–1521.

17 Y. Xue, S. Datta and M. A. Ratner, *J. Chem. Phys.*, 2001, **115**, 4292–4299.

18 S. Datta, *Quantum Transport: Atom to Transistor*, Cambridge University Press, Cambridge, 2005.

19 J. M. Seminario, *Molecular and Nano Electronics: Analysis, Design and Simulation Vol. 17*, Elsevier, Amsterdam, 2006.

20 P. Hohenberg, and W. Kohn, *Phys. Rev.*, 1964, **136**, B864.

21 W. Kohn and L. J. Sham, *Phys. Rev.* 1965, **140**, A1133.

22 M. Brandbyge, J.-L. Mozos, P. Ordejón, J. Taylor and K. Stokbro, *Phys. Rev. B*, 2002, **65**, 165401.

23 K. Stokbro, J. Taylor, M. Brandbyge, J.-L. Mozos and P. Ordejón, *Comput. Mater. Sci.,* 2003, **27**, 151–160.

24 K. Stokbro, *J. Phys.: Condens. Matter*, 2008, **20**, 064216/1–7.

25 N. D. Lang and Ph. Avouris, *Phys. Rev. B*, 2001, **64**, 125323–125329.

26 P. A. Derosa and J. M. Seminario, *J. Phys. Chem. B*, 2001, **105**, 471–481.

27 J. Heurich, J. C. Cuevas, W. Wenzel and G. Schön, *Phys. Rev. Lett.*, 2002, **88**, 256803–256806.

28 R. Stowasser and R. Hoffmann, *J. Am. Chem. Soc.*, 1999, **121**, 3414–3420.

29 R. van Meer, O. V. Gritsenko and E. J. Baerends, *J. Chem. Theory Comput.* 2014, **10**, 4432−4441.

30 T. Tada and K. Yoshizawa, *ChemPhysChem*, 2002, **3**, 1035–1037.

31 T. Tada and K. Yoshizawa, *J. Phys. Chem. B*, 2003, **107**, 8789–8793.

32 T. Tada and K. Yoshizawa, *J. Phys. Chem. B*, 2004, **108**, 7565–7572.

33 K. Yoshizawa, T. Tada and A. Staykov, *J. Am. Chem. Soc.*, 2008, **130**, 9406–9413.

34 Y. Tsuji, A. Staykov and K. Yoshizawa, *J. Phys. Chem. C*, 2009, **113**, 21477–21483.

35 X. Li, A. Staykov and K. Yoshizawa, *J. Phys. Chem. C*, 2010, **114**, 9997–10003.

36 X. Li, A. Staykov and K. Yoshizawa, *Theor. Chem. Acc.*, 2011, **50**, 6200–6209.

37 Y. Tsuji, A. Staykov, and K. Yoshizawa, *J. Am. Chem. Soc.*, 2011, **133**, 5955–5960.

38 T. Tada, T. Yamamoto and S. Watanabe, *Theor. Chem. Acc.*, 2011, **130**, 775–788.

39 K. Yoshizawa, *Acc. Chem. Res.*, 2012, **45**, 1612–1621.

40 X. Li, A. Staykov and K. Yoshizawa, *Bull. Chem. Soc. Jpn.*, 2012, **85**, 181–188.

41 M. Taniguchi, M. Tsutsui, R. Mogi, T. Sugawara, Y. Tsuji, K. Yoshizawa and T. Kawai, *J. Am. Chem. Soc.*, 2011, **133**, 11426–11429.

42 T. Morikawa, S. Narita and D. J. Klein, *Chem. Phys. Lett.* 2005, **402**, 554–558.

43 G. C. Solomon, D. Q. Andrews, T. Hansen, R. H. Goldsmith, M. R. Wasielewski, R. P. van Duyne and M. A. Ratner, *J. Chem. Phys.*, 2008, **129**, 054701/1–8.

44 G. C. Solomon, D. Q. Andrews, R. H. Goldsmith, T. Hansen, M. R. Wasielewski, R. P. van Duyne and M. A. Ratner, *J. Am. Chem. Soc.*, 2008, **130**, 17301–17308.

45 S.-H. Ke and W. Yang, *Nano Lett.*, 2008, **8**, 3257–3261.

46 P. W. Fowler, B. T. Pickup, T. Z. Todorova and W. Myrvold, *J. Chem. Phys.* 2009, **131**, 244110.

47 D. Nozaki, H. M. Pastawski and G. Cuniberti, *New. J. Phys.*, 2010, **12**, 063004.

48 M. Mardaani, H. Rabani and A. Esmaeili, *Solid State Commun.* 2011, **151**, 928–932.

49 D. Nozaki, H. Sevinçli, S. M. Avdoshenko, R. Gutierrez and G. Cuniberti, *Phys. Chem.*

Chem. Phys., 2013, **15**, 13951–13958.

50 Y. Okuno and T. Ozaki, *J. Phys. Chem. C*, 2013, **117**, 100–109.

51 Y. Tsuji and R. Hoffmann, *Angew. Chem. Int. Ed.*, 2014, **53**, 4093–4097.

52 Y. Tsuji, R. Hoffmann, R. Movassagh and S. Datta, *J. Chem. Phys.*, 2014, **141**, 224311.

53 K. G. L. Pedersen, M. Strange, M. Leijnse, P. Hedegård, G. C. Solomon and J. Paaske, *Phys. Rev. B*, 2014, **90**, 125413.

54 D. Nozaki, S. M. Avdoshenko, H. Sevinçli and G. Cuniberti, *J. Appl. Phys.*, 2014, **116**, 074308.

55 Y. –H. Zhou, C. –Y. Chen, B. –L. Li and K. –Q. Chen, *Carbon*, 2015, **95**, 503–510.

56 S. A. Tawfik, X. Y. Cui, S. P. Ringer and C. Stampfl, *J. Chem. Theory Comput.*, 2015, **11**, 4154−4158.

57 D. Nozaki, Lokamani, A. Santana-Bonilla, A. Dianat, R. Gutierrez and G. Cuniberti, *J. Phys. Chem. Lett.*, 2015, **6**, 3950−3955.

58 D. Fracasso, H. Valkenier, J. C. Hummelen, G. C. Solomon and R. C. Chiechi, *J. Am. Chem. Soc.*, 2011, **133**, 9556–9563.

59 N. Darwish, I. Díez-Pírez, P. Da Silva, N. Tao, J. J. Gooding and M. N. Paddon-Row, *Angew. Chem.*, 2012, **124**, 3257 –3260.

60 S. Ballmann, R. Härtle, P. B. Coto, M. Elbing, M. Mayor, M. R. Bryce, M. Thoss and H. B. Weber, *Phys. Rev. Lett.*, 2012, **109**, 056801.

61 S. V. Aradhya, J. S. Meisner, M. Krikorian, S. Ahn, R. Parameswaran, M. L. Steigerwald, C. Nuckolls and L. Venkataraman, *Nano Lett.*, 2012, **12**, 1643–1647.

62 C. M. Guédon, H. Valkenier, T. Markussen, K. S. Thygesen, J. C. Hummelen and S. J. van

der Molen, *Nature Nanotechnol.*, 2012, **7**, 305–309.

63 K. Fukui, *Theory of Orientation and Stereoselection*, Springer, Berlin, 1970.

64 R. B. Woodward and R. Hoffmann, *The Conservation of Orbital Symmetry*, Verlag Chemie GmbH, Weinheim, 1970.

65 M. J. S. Dewar, *The Molecular Orbital Theory of Organic Chemistry*, McGraw-Hill, New York, 1969.

66 C. Caroli, R. Combescot, P. Nozieres and D. Saint-James, *J. Phys. C*, 1971, **4**, 916–929.

67 R. Combescot, *J. Phys. C*, 1971, **4**, 2611–2622.

68 S. Priyadarshy, S. S. Skourtis, S. M. Risser and D. N. Beratan, *J. Chem. Phys.*, 1996, **104**, 9473–9481.

69 The orbital rule was obtained for coherent quantum transport in π-conjugated molecular junctions by assuming the three conditions: weak coupling with electrodes, electron-hole symmetry, and the Fermi level located in the midgap of HOMO and LUMO. These are discussed in Ref. 39 from the viewpoint of orbital energy. The applicable range of the rule can be extended to a wider region by making a different matrix expression by using different bases (e.g., atomic orbital (present case), molecular orbital, or spin-spin direct product bases). For example, the constructive/destructive interference was found in a spin transport including spin-flip processes in a tight-binding chain, and the quantum interference depending on the spin-flip processes was explicitly explained with the orbital rule by using the matrix similarity in both cases. See details in Ref. 38.

70 S. Md. Pratik and A. Datta, *Phys.Chem. Chem. Phys.*, 2013, **15**, 18471–18481.

71 P. Sautet and C. Joachim, *Chem. Phys. Lett.*, 1988, **153**, 511−516.

72 T. Tada, D. Nozaki, M. Kondo, S. Hamayama and K. Yoshizawa, *J. Am. Chem. Soc.*, 2004, **126**, 14182–14189.

73 G. Sedghi, V. M. García-Suárez, L. J. Esdaile, H. L. Anderson, C. J. Lambert, S. Martín, D. Bethell, S. J. Higgins, M. Elliott, N. Bennett, J. E. Macdonald and R. J. Nichols, *Nature Nanotechnol.*, 2011, **6**, 517–523.

74 P. Moreno-García, M. Gulcur, D. Z. Manrique, T. Pope, W. Hong, V. Kaliginedi, C. Huang, A. S. Batsanov, M. R. Bryce, C. Lambert and T. Wandlowski, *J. Am. Chem. Soc.*, 2013, **135**, 12228–12240.

75 Since the orbital rule points out the importance of molecular orbital phases and amplitudes at the connecting atoms with electrodes, one might be wondering why orbital delocalization is required. This point is simply explained in the following hypothetical system where HOMO and LUMO are perfectly localized at the two edge atoms, and the phase relations on the two atoms for HOMO and LUMO are respectively (+ +) and (+ −), the constructive interference case. In such a system, the perfect localization at the edge two atoms in the frontier orbitals means that the HOMO and LUMO have an identical orbital energy. Once the two orbitals are energetically degenerated, we can execute a unitary transformation using the two frontier orbitals, and we get other representations for HOMO and LUMO in which the orbital amplitude is confirmed only at a single edge atom, (e.g., HOMO/LUMO is localized at the left-/right-edge atom). Thus Green's function that requires two orbital coefficients of the connecting two atoms will be zero. That is why orbital delocalization is required in order to have different orbital energies for HOMO and LUMO.

76 M. Kiguchi, T. Takahashi, Y. Takahashi, Y. Yamauchi, T. Murase, M. Fujita, T. Tada and S. Watanabe, *Angew. Chem. Int. Ed.*, 2011, **50**, 5708–5711.

77 M. Kiguchi, J. Inatomi, Y. Takahashi, R. Tanaka, T. Osuga, T. Murase, M. Fujita, T. Tada and S. Watanabe, *Angew. Chem. Int. Ed.*, 2013, **52**, 6202–6205.

78 S. Fujii, T. Tada, Y. Komoto, T. Osuga, T. Murase, M. Fujita and M. Kiguchi, *J. Am. Chem. Soc.*, 2015, **137**, 5939–5947.

79 P. Delaney and J. C. Greer, *Int. J. Quantum. Chem.*, 2004, **100**, 1163–1169.

80 P. Delaney and J. C. Greer, *Phys. Rev. Lett.*, 2004, **93**, 036805.

81 C. Toher, A. Filippetti, S. Sanvito and K. Burke, *Phys. Rev. Lett.*, 2005, **95**, 146402.

82 C. Toher and S. Sanvito, *Phys. Rev. Lett.*, 2007, **99**, 056801.

83 P. Darancet, A. Ferretti, D. Mayou and V. Olevano, *Phys. Rev. B*, 2007, **75**, 075102.

84 K. S. Thygesen and A. Rubio, *J. Chem. Phys.*, 2007, **126**, 091101.

85 T. Tada, M. Kondo and K. Yoshizawa, *J. Chem. Phys.*, 2004, **121**, 8050–8057.

86 T. Tada, S. Hamayama, M. Kondo and K. Yoshizawa, *J. Phys. Chem. B*, 2005, **109**, 12443–12448.

87 X. Xiao, B. Xu and N. J. Tao, *Nano Lett.*, 2004, **4**, 267.

88 Y. Kim, T. Pietsch, A. Erbe, W. Belzig and E. Scheer, *Nano Lett.*, 2011, **11**, 3734–3738.

89 Recent experimental studies on molecular conductance of the BDT junction reveal that three or more contact configurations are related to experimentally observed conductance of BDT. However, in the present study, the BDT junction with the hollow site adsorption was adopted for comparison between the theoretical calculation and experimental observation because the hollow site adsorption of BDT is the most energetically stable

configuration.

90 L. Venkataraman, J. E. Klare, C. Nuckolls, M. S. Hybertsen and M. L. Steigerwald, *Nature*, 2006, **442**, 904–907.

91 S. Y. Quek, L. Venkataraman, H. J. Choi, S. G. Louie, M. S. Hybertsen and J. B. Neaton, *Nano Lett.*, 2007, **7**, 3477–3482.

92 A. D. Becke, *J. Chem. Phys.*, 1993, **98**, 5648.

93 C. Lee, W. Yang and R. G. Parr, *Phys. Rev. B*, 1988, **37**, 785.

94 T. H. Dunning, Jr. and P. J. Hay, *Modern Theoretical Chemistry*, Plenum, New York, Vol. 3, p.1, 1976.

95 W. R. Wadt and P. J. Hay, *J. Chem. Phys.,* 1985, **82**, 284.

96 W. R. Wadt and P. J. Hay, *J. Chem. Phys.*,1985, **82**, 299.

97 J. M. Soler, E. Artacho, J. D. Gale, A. García, J. Junquera, P. Ordejón and D. Sánchez-Portal, *J. Phys.: Condens. Matter*, 2002, **14**, 2745–2779.

98 ATK Manual ATK version 12.8.0; QuantumWise A/S:Copenhagen, Denmark; http://www.quantumwise.com.

99 J. P. Perdew, K. Burke and M. Ernzerhof, *Phys. Rev. Lett.*, 1996, **77**, 3865–3868.

100 Y. Tsuji, A. Staykov and K. Yoshizawa, *J. Phys. Chem. C*, 2012, **116**, 2575–2580.

101 S. Lakshmi, A. Datta and S. K. Pati, *Phys. Rev. B*, 2005, **72**, 045131.